

High-Fidelity VLA Imaging of the Radio Structure of 3C273

R. A. Perley¹ and K. Meisenheimer²

¹ National Radio Astronomy Observatory
Socorro NM 87801
e-mail: rperley@nrao.edu

² Max Planck Institut für Astronomie
Heidelberg, Germany

ABSTRACT

Context. 3C273, the nearest bright quasar, comprises a strong nuclear core and a bright, one-sided jet extending ~ 23 arcseconds to the SW. The source has been the subject of imaging campaigns in all wavebands. Extensive observations of this source have been made with the Very Large Array and other telescopes as part of a campaign to understand the jet emission mechanisms. Partial results from the VLA radio campaign have been published, but to date, the complete set of VLA imaging results has not been made available.

Aims. We have utilized the VLA to determine the radio structure of 3C273 in Stokes I, Q, and U, over the widest possible frequency and resolution range.

Methods. The VLA observed the source in all four of its configurations, and with all eight of its frequency bands, spanning 73.8 MHz to 43 GHz. The data were taken in a pseudo-spectral line mode to minimize the VLA's correlator errors, and were fully calibrated with subsequent self-calibration techniques to maximise image fidelity.

Results. Images in Stokes parameters I, Q, and U, spanning a resolution range from 6 arcseconds to 88 milliarcseconds are presented. Spectral index images, showing the evolution of the jet component are shown. Polarimetry demonstrates the direction of the magnetic fields responsible for the emission, and rotation measure maps show the RM to be very small with no discernible trend along or across the jet. This paper presents a small subset of these images to demonstrate the major characteristics of the source emission. A library of all ~ 500 images has been made available for open, free access by interested parties.

Key words. radio astronomy – quasars

1. Introduction

3C273 (J1229+0203), the first identified quasar (Schmidt 1963), is one of the closest and most luminous of all quasars. Imaging of this source shows that at all wavebands, 3C273 comprises a bright, flat-spectrum nucleus with highly variable flux density, and a one-sided, highly polarized, narrow jet extending ~ 23 arcseconds to the SW of the nucleus. Since its discovery, and due to its relative proximity ($z = 0.158$, so 3.4 arcsecond ~ 1 kpc) and angular size, 3C273 has been observed by a wide range of instruments from long-wavelength radio through X-ray.

3C273 was the target of an extensive and comprehensive observational campaign spanning many wavebands and utilizing many telescopes from 1995 through 2005. Key results from this campaign are to be found in Jester et al. (2005), and references within, which presents results from observations made with the VLA from 8 through 43 GHz, along with HST observations from the near-ultraviolet through near-infrared. However, the radio images shown in this paper are a small selection of those available from the suite of VLA observations of this source.

The purpose of this paper is to present an overview of the key results from all the VLA imaging of 3C273, from the data taken between 1987 and 1999.

2. Observations

The results presented here are from three separate observational campaigns utilizing the Very Large Array¹, each with different goals. The first, taken in 1987, 1991 and 1999 under project codes AP134, AB608, and AB916 was intended to search for changes in the structure of the radio jet over the 14-year span of time. The second, in 1995 through 1997, under project codes AR334 and AR371, were part of a full coverage study of the jet emission properties. Neither of these projects included observations from the low frequency bands, at 73.8 and 327 MHz. The results included in this paper from these bands are taken from project AK461, whose goal was to demonstrate the imaging capability of the VLA at low frequencies by observing a selection of 3C sources, including 3C273.

The observing details for all these projects are given in Table 1. To minimize the baseline-based errors ('closure errors') which limit image fidelity for very bright sources such as 3C273, we employed the spectral line mode '1A', providing 64 channels in a single correlation over 12.5 MHz bandwidth, or 'PA' with a bandwidth of 12.5 MHz, providing all four complex correlations with 16 channels each. The low frequency observations were taken in a dual frequency mode, providing only the parallel hand correlations in spectral line mode '4', with 3.125 MHz bandwidth at 327 MHz, and 1.56 MHz bandwidth at 73.8 MHz.

¹ The National Radio Astronomy Observatory is a facility of the National Science Foundation operated under cooperative agreement by Associated Universities, Inc.

Table 1. VLA Observing Log

Project	Date	Config.	Bands ^a	Duration(hr)
AP134	07 Sep 1987	A	C, U	12
AP134	10 Sep 1987	A	C, U	12
AB608	04 Jul 1991	A	C, U	12
AB608	14 Jul 1991	A	C, U	12
AR334	09 Jul 1995	A	L,C,X,U,K,Q	12
AR334	13 Oct 1995	B	L,C,X,U,K,Q	12
AR334	01 Mar 1996	C	L,C,X,U,K,Q	12
AR371	08 Nov 1997	D	L,C,X,U,K,Q	6
AK461	07 Mar 1998	A	4,P	24
AB916	19 Jun 1999	A	C, U	10

^a 4: 73.8 MHz, P: 327 MHz, L: 1365 MHz, C: 4885 MHz, X: 8415 MHz, U: 14965 MHz, K: 22485 MHz, Q: 43315 MHz

Table 2. Flux Density of 3C286

Band	Freq MHz	Flux Density Jy
P	327	25.0
L	1365	15.02
C	4885	7.410
X	8415	5.197
U	14915	3.455
K	22485	2.574
Q	43315	1.537

Because 3C273 is a very strong radio source with a nuclear core suitable for calibration, a special calibration regimen was adopted. At the lower frequencies (1365 MHz, 4885 MHz, and 8415 MHz), where the jet emission is significant and the array resolution lower, phase and amplitude calibration were accomplished with the nearby unresolved source J1150–0023. At the higher frequency bands (14965 MHz, 22485 MHz, and 43315 MHz), this secondary calibrator was not necessary, and the nuclear component of 3C273 itself provided the calibration.

The observations for the primary projects AR334 and AR371 were arranged on an hourly cycle, within which the first 17 minutes were used for the observations at the lowest three frequencies (including the calibrator), followed by 10 minutes of 14965 MHz, 12 minutes at 22485 MHz, and 15 minutes at 43315 MHz. This variation of duration with frequency was done to offset the loss of sensitivity at the higher frequency bands. Referenced pointing, a technique which determines the local pointing offsets, was done utilizing 3C273 at X-band, with the corrections applied to the subsequent observations at higher frequencies.

The VLA’s 40 – 50 GHz system (Q-band) was being implemented during this program, with the result that only 9, 11, 13, and 13 antennas were outfitted for the A, B, C, and D configuration observations, respectively. As this system was in its early stages, and because we did not expect to be able to accomplish detailed structure studies with the incomplete system, we observed only every other hour at this band.

The flux density scale was set through an observation of 3C286, the VLA’s primary flux density calibrator, at the end of each observing run. The values used were from Perley & Butler (2013), which are based on the Baars et al. (1966) for the frequencies below 2 GHz, and on quantitative emission models of Mars for the high frequencies. The values utilized are shown in Table 2.

Calibration of the data was done using the AIPS software package, using the following procedure:

1. Quick inspection of the amplitude data was used to remove obviously bad data from ‘dead’ antennas.
2. The bandpass functions for the polarizations observed were determined using 3C273 itself, using BPASS.
3. The spectral channel data were corrected by the bandpass, and collapsed to a single ‘pseudo-continuum’ channel, using SPLAT. The result is a single-frequency, multi-source database, similar to what the continuum system provides, but with much reduced baseline-dependent (‘closure’) errors.
4. As 3C286 is partially resolved to most configurations at all frequencies, our observations of this source were used to construct a source model whose brightness scale was adjusted to give the correct total flux density given in Table 2.
5. These models of 3C286 were then used by CALIB to determine the antenna gains, and to derive the flux density of the calibration source J1150–0023 at L, C, and X bands. For the higher frequencies, the flux density of 3C273 was derived directly, using the longer spacings for which the nuclear core is cleanly separable.
6. For the higher frequency observations, the elevation dependency of the antenna gains was determined by ELINT, with the resulting dependencies applied to the data from all sources.
7. The time-variable complex gains (amplitude and phase) were then derived, using 1150–003 for L, C, and X bands, and using 3C273 itself for U, K, and Q bands via CALIB, and applied using CLCAL.
8. The polarization calibration program PCAL was used to determine the antenna polarization.
9. The RCP - LCP phase difference was determined by observation of the plane of polarized flux for 3C286, and applied to the data using CLCOR.
10. The data were then split out by source into individual files, applying all gains, for subsequent self-calibration and imaging, using AIPS program SPLIT.

Calibration of the 73.8 and 327.5 MHz data followed a similar procedure (minus the polarization calibration stage), except that at 327.5 MHz, the phase calibration was based on the global average of observations of 3C286, 3C147, 3C48, and 3C138, while at 73.8 MHz, only Cygnus A was used for calibration.

All subsequent calibration was done on a single-source basis, separately for each frequency and configuration, utilizing well-established methodologies of self-calibration. For sources like 3C273, comprising simple structures with sharp brightness gradients, these procedures are especially effective. Although the use of the spectral line correlator modes reduced the ‘closure’² errors to very small values – typically to 0.1% and 0.05 degrees – a baseline-based calibration step, using the AIPS program BLCAL, was done for some of the frequency/configuration databases, if the characteristic sign of the effect of these errors was seen in any map³

Self-calibration was done for each frequency and configuration separately. Following this, the databases from different configurations were combined to permit imaging over a very wide range of spatial scales, and to provide the best dynamic range and sensitivity at each frequency. Because the nuclear source of

² These are defined as baseline-based errors which cannot be factored out by antenna.

³ For a source located near the equatorial plane, like 3C273, these errors are manifested as a vertical disturbance up the center of the image.

Table 3. Flux Density and Polarization Variability of 3C273

Date		L	C	X	U	K	Q
		1365	4885	8415	14965	22345	43340
09/07/95	I	32.7	36.0	33.0	28.4	23.8	20.0
	χ	-27	-23	-26	-21	-35	-19
	%	0.9	3.0	3.4	5.6	4.3	4.6
03/10/95	I	32.8	35.6	30.0	24.3	19.8	16.1
	χ	-28	-21	-26	-24	-29	-32
	%	1.0	3.1	3.0	5.8	6.0	3.4
01/03/96	I	31.7	36.1	26.9	22.3	24.3	30.8
	χ	-34	-23	-26	-30	-40	-40
	%	0.8	3.0	4.2	6.1	4.1	2.9
01/11/97	I		29.6	26.7	31.5	35.6	37.7
	χ		-23	-26	-33	-36	-38
	%		3.1	4.7	3.2	2.8	2.1

3C273 is variable, and the observations for AR334 and AR371 were taken over 2.5 year timescale, the flux density of the nuclear emission (in all three Stokes' parameters) had to be adjusted to a common value before combination. This was done using the AIPS program UVMOD, using the A-configuration values as the reference. The flux densities and polarizations of the nucleus, as a function of time and frequency, are given in Table 3.

3. Imaging

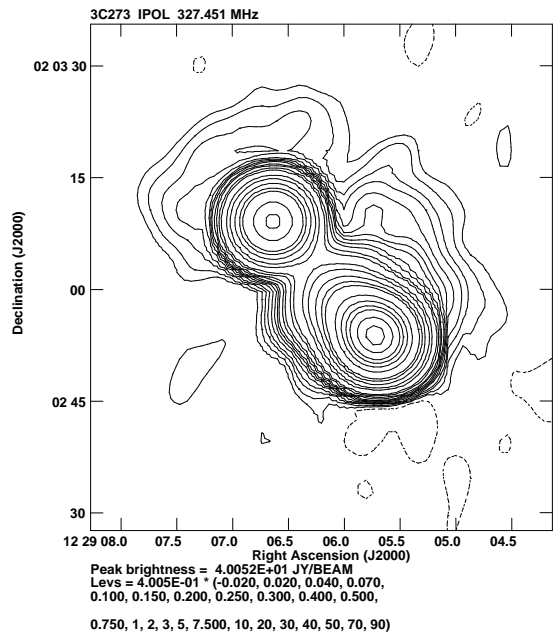
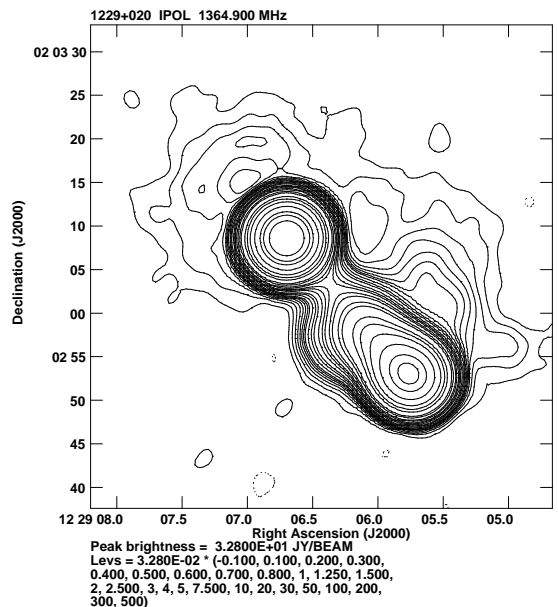
We present here images of the structure of 3C273, with resolutions chosen to highlight the major structural components of the source.

Low resolution images of the source at ~ 5 arcseconds resolution at P, L, and C bands show the presence of a previously unknown diffuse component of emission. This emission is of approximate extent 30 by 45 arcseconds, centered approximately 10 arcseconds (or 3 kpc) to the north of the brighter core and jet emission, and aligned with the jet axis. Figure 1 shows the structure at 327 MHz, with 6 arcsecond resolution, figures 2 and 3 show the structure at 1365 MHz and 4885 MHz with 4 arcseconds resolution. Imaging at 1465 MHz with 15 arcseconds resolution shows no other extended emission to our brightness sensitivity level of ~ 0.6 mJy/beam.

The extended emission to the north-west is unpolarized to a level of ~ 0.1 mJy/beam, implying a maximum fractional polarization of $<5\%$. The brighter extended emission, immediately to the north of the jet shows a marginal detection of polarized flux, with a maximum fraction of $\sim 10\%$.

The images made at this resolution clearly show the halo at the lowest three frequencies (327, 1465, and 4885 MHz). The differences in the halo brightness distribution apparent between Figures 1 and 2 should not be interpreted as evidence for significant spectral variations, as the process of self-calibration, and in particular, that of baseline-based calibration, are likely to have generated these variations. We do, however, believe the detection of the halo to be secure.

The three major components – core, jet, and halo, can be separated by suitable integration of the image brightness, with the resulting total flux densities for these components given in Table 4. We emphasize that these values of the halo flux are approximate – a 30% error should be assumed. This extended halo of emission – unknown before these observations – may represent the lobes of a low-luminosity ‘FR1’ radio source. In this interpretation, the nuclear core and the one-sided jet represent Doppler-brightened emission from a relativistic flow aligned


Fig. 1. 3C273 at 327 MHz, with 6 arcsecond resolution. The extended halo emission, slightly offset from the bright emission, is clearly visible.

Fig. 2. 3C273 at 1365 MHz, with 4 arcsecond resolution. The extent of the halo is similar to that at 327 MHz, although the details of the emission differ somewhat.

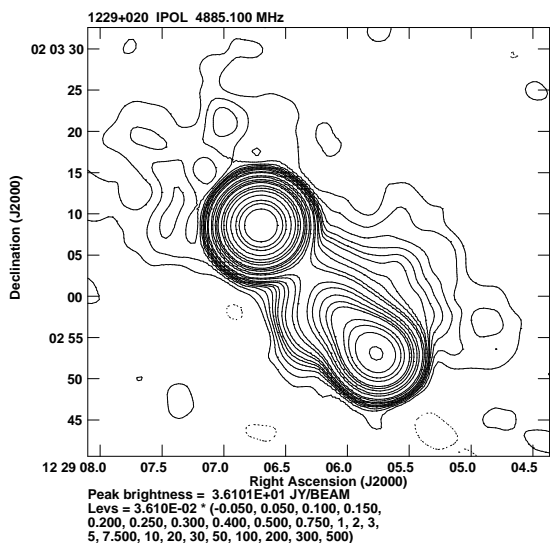


Fig. 3. 3C273 at 4885 MHz, with 4 arcsecond resolution. The overall extent of the diffuse emission is similar to that at 327 and 1365 MHz, but the details differ, most likely due to variations introduced by the calibration and imaging process.

Table 4. Core and Extended Flux Densities for 3C273

Frequency MHz	Core Jy	Jet Jy	Halo Jy
73.8	9.1	151.5	?
327.5	12.7	52.8	0.80
1365	32.80	17.2	0.30
4885	36.10	5.75	0.15
8415	33.12	3.49	0.04

close to the line of sight. This interpretation is explored by Punsly & Kharb (2016).

It will be noted from Figures 1 and 2 that there is a modest ‘bulge’ of emission on the southern side of the source, about midway down the jet. This structure, which was previously seen by imaging with MERLIN, is more clearly shown at 2 arcsecond resolution, in Figure 4. In Figure 5 we show the linear polarization of the emission at a 2 arcsecond resolution at 1365 MHz.

Increasing the resolution by another factor of two resolves out the extended emission completely, and reveals detailed structures of the jet emission itself. Figure 6 shows the emission with 1 arcsecond resolution at 14965 MHz. Notable here is the presence of a bright, straight, apparently unresolved inner jet, extending halfway between the nuclear core and well-resolved outer jet.

The inner jet has previously been detected in observations by MERLIN (Davis et al. 1985) and the VLA (Conway et al. 1993), but with poorer sensitivity that the results shown here.

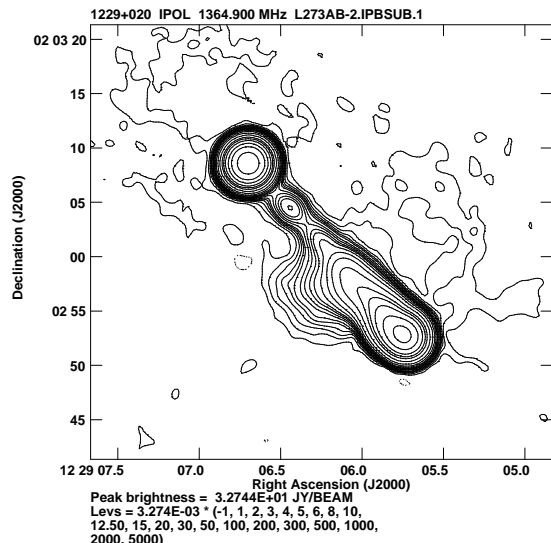


Fig. 4. 3C273 at 1365 MHz, with 2 arcsecond resolution. The inner and outer jets are now visible, while the faint halo is now nearly resolved out. The brighter extension to the SE of the outer jet is clearly visible.

Optical emission from this inner jet has been reported from HST observations by Martel et al. (2003).

Figure 7 shows the polarization at 8415 MHz with 1 arcsecond resolution. The inner jet polarization is quite low, typically 5 to 10 %, with the B-field direction along the jet. The outer jet shows considerable variation in polarization structure, with a high degree of polarization (~30%) along the edges, and much lower values throughout the center.

The structures of the inner and outer jets are strikingly different, as illustrated in a very deep image, taken at 4866 MHz, with 0.4 arcsecond resolution, shown in Figure 8. Some important features of the jet structure seen in the figure are noted here:

- The inner jet is nearly straight, and is transversely unresolved for the first 13 arcseconds of its length.
- There are three elongated enhancements in brightness along this inner portion, separated by 5 arcseconds.
- These three elongated enhancements are not perfectly colinear – the outer two are tilted, in opposite directions, by about 5 degrees. The innermost enhancement is perfectly colinear with the brightest hotspot near the end of the outer jet.
- An emerging, unresolved, knot of emission is seen 550 milliarcseconds outside the nuclear position. This structure is to be identified with the innermost jets seen on milliarcsecond scales by the VLBA by Zavala & Taylor (2005)
- The inner jet abruptly transitions to a wider (~3 arcseconds) outer jet, 13 arcseconds from the nucleus.
- The outer jet exhibits considerable variations in structure, including an oscillatory center brightness with 6 arcseconds period, and ~1 arcsecond amplitude.

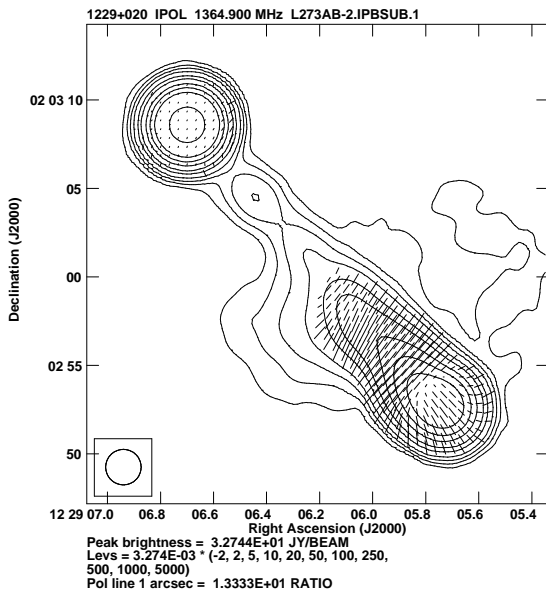


Fig. 5. The polarization of 3C273 at 1365 MHz with 2 arcsecond resolution. The plotted E-vectors show the orientation of the plane of linear polarization, their lengths are proportional to the degree of polarization. The observed pattern shows that the projected magnetic field is along the jet, and wraps around the end. This pattern, with the B-field aligned with the edges of the emission, is the general rule for synchrotron-emitting extragalactic radio sources. The extended emission to the SE of the jet is polarized at a level at or less than 15%.

- There is a prominent knot (‘H2’) of emission oriented transverse to the jet axis, 22 arcseconds from the nucleus. Emission is detected for two more arcseconds beyond this knot (‘H1’).

The oscillatory behavior of the central spine of emission within the outer jet is more clearly seen with 0.25 arcsecond resolution at 14.9 GHz, as shown in Figure 9

At 125 milliarcsecond resolution, more details of the brighter components of the jet become visible. The innermost jet is clearly visible, as shown in Figure 10. No polarized flux from this inner jet was detected, as the noise level in this region is near 5 mJy/beam – comparable to the jet brightness. The outer jet, at this same resolution, is seen in Figure 11

The detailed polarization image at 0.25 arcsecond resolution shows a considerably more complex structure than in total intensity, as shown in Figure 12. The polarization fraction is generally low in the interior regions of the jet, and reaches high values – as high as 55% – along the boundaries. The projected magnetic field accurately follows the total intensity boundaries of the jet. At 0.125 arcseconds resolution, the only detectable polarization emission at 14.9 GHz is from the brightest structures associated with the hotspot, as shown in Figure 13. The degree of polarization in general remains relatively low in these bright areas – typically 10%, but reaches ~40% at the bright hotspot, with a magnetic field orientation perpendicular to the jet main axis.

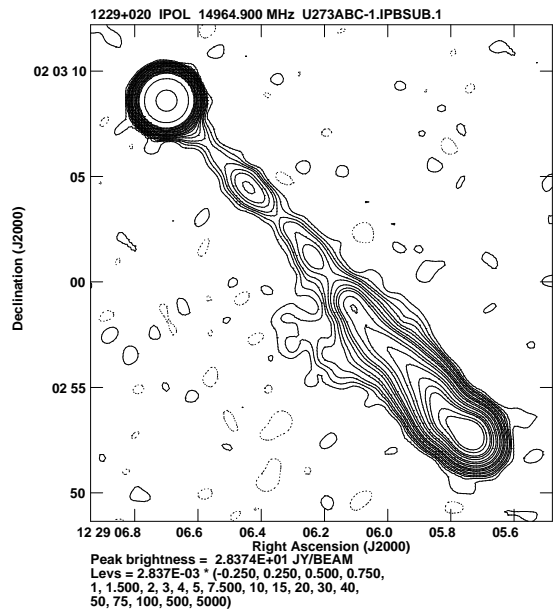


Fig. 6. 3C273 at 14965 MHz, with 1 arcsecond resolution. The extended emission is nearly resolved out, while details of the inner jet are becoming clear.

Concluding this section on the structure of the jet, we show our highest resolution image – 88 milliarcseconds at 22345 MHz – in Figure 14. The bright hotspot is now fully resolved. No polarized emission is detected, due to insufficient surface brightness sensitivity.

4. Spectral Index

We show, in Figure 15 a four-panel spectral index image⁴ at 2.0 arcsecond resolution, spanning 1.365 through 22.3 GHz.

Figure 15 shows that the inner jet has a spectral index near 0.65, and that the outer jet has a uniform spectral index near 0.85. There is a notable steepening of the radio spectral index in the vicinity of the brightest hotspot, to -1.0, between 14965 and 22485 MHz. The spectral index in the hotspot vicinity at higher frequencies continues to steepen, reaching between 22.3 approximately $\alpha_{23345}^{43340} \sim 1.4$ between 23.3 and 43.3 GHz.

The steeping of the spectrum is not a property of the brightest hotspot only, however, as is made clear in Figure 16, showing the spectral index images between X and K bands at 0.25 arcseconds resolution.

The spectral index of the low-brightness extended emission to the north and east could not be determined, as the intensity is too low to permit an accurate image. However, the integrated fluxes shown in Table 4 can be used to provide a rough measure of $\alpha \sim 0.6$.

The interpretation of these spectral trends is beyond the scope of this paper. We refer the reader to the thorough discus-

⁴ Defined as $\alpha = (\log(B_1) - \log(B_2)) / (\log(\nu_2) - \log(\nu_1))$.

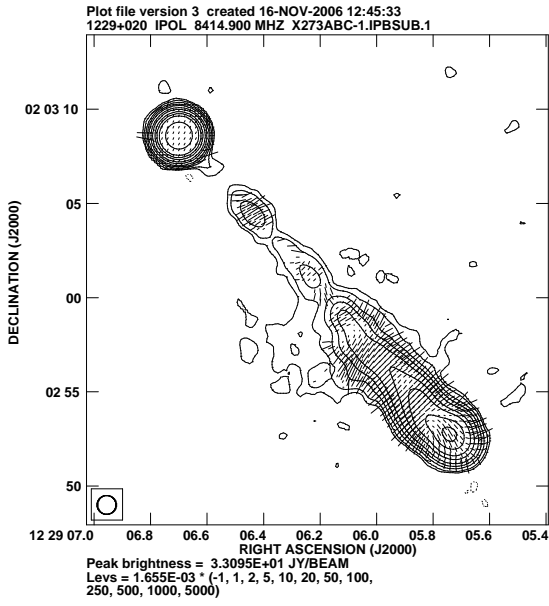


Fig. 7. The polarization of 3C273 at 8415MHz, with 1 arcsecond resolution. The projected magnetic field orientation is orthogonal to these plotted E-vectors, and accurately follows the brightness isocontours.

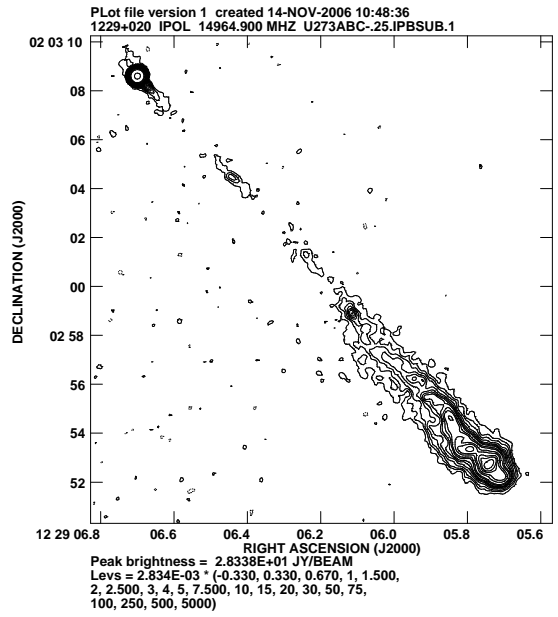


Fig. 9. 3C273 at 14965 MHz, with 0.25 arcsecond resolution. The oscillatory structure of the outer jet is now more clearly evident.

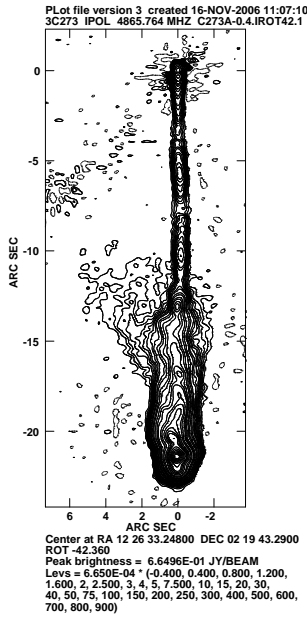


Fig. 8. 3C273 at 4865 MHz and 0.40 arcsecond resolution, rotated CW by 42.36 degrees. The unresolved nuclear component has been removed, leaving a 30 mJy residual at the top to mark the nuclear position. Notable here is the high brightness of the inner jet, which is transversely unresolved.

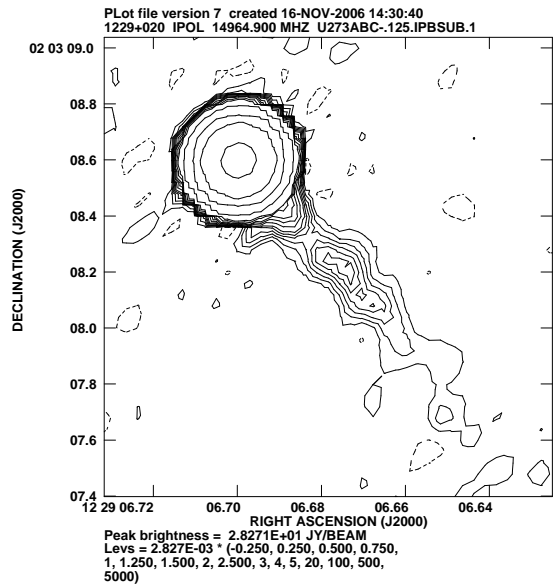


Fig. 10. The innermost jet, as seen at 14965 MHz, with 125 milliarsecond resolution. The 'bulge' in emission immediately to the SW of the nucleus is the end of the milliarsecond-scale jet.

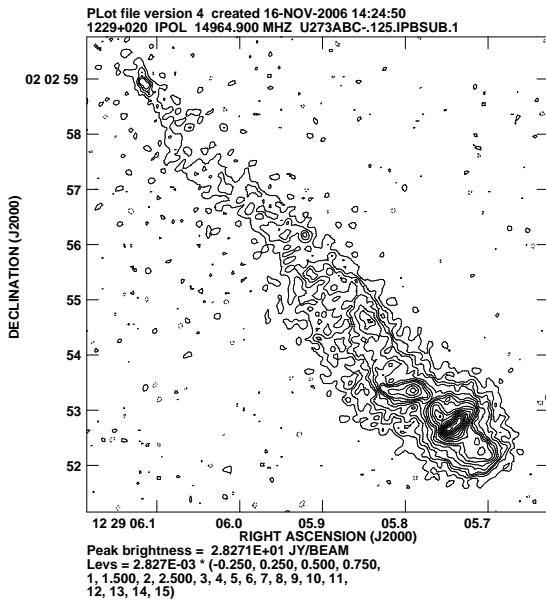


Fig. 11. The brightest portions of the outer jet, showing the brightest hotspot, and the oscillatory ridge leading to it.

sion given in Jester et al. (2005), which incorporates observations extending from the radio through the ultraviolet.

Finally, we note that the polarization images allow a determination of the rotation measure. The most sensitive measure is between the lowest pair of frequencies, 1365 and 4885 MHz. Figure 17 shows the RM at 1.4 arcseconds resolution. The RM of the entire outer jet is uniform, with mean value 3.7 rad/m^2 , with a dispersion of only 1.7 rad/m^2 . There is no discernible gradient either across, or along the jet. The RM of the nucleus is slightly less: -2.0 rad/m^2 .

5. Image Archive

The results shown here are a small fraction of the approximately 500 images available from this project. We have placed the full suite of images, in FITS format, in a publically accessible ftp site. To access by anonymous ftp, go to 'ftp.aoc.nrao.edu', and change directory to 'pub/staff/rperley/3C273'. The images are named in a manner which provides sufficient information to identify the content. In general, files are named thusly:

bb273cccc-rr.type

where

- 'bb' are the band(s) utilized for the image
- 'cccc' are the configurations utilized
- 'rr' is the resolution of the restoring beam, in arcseconds.
- 'type' is the type of image.

There are many possibilities for 'type'. These include:

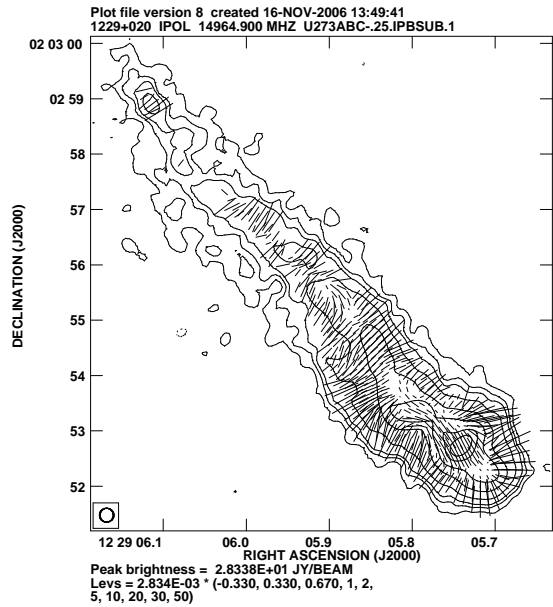


Fig. 12. The polarization structure of the outer jet at 14965 MHz, with 0.25 arcsecond resolution. The length of the vectors indicates the fractional linear polarization. Their orientation is perpendicular to the projected jet magnetic field.

- A leading 'I', 'Q' or 'U' denotes the polarization. This is normally followed by 'CLN', denoting a deconvolved image. If followed by 'SUB', the image is a subsection of the original (deconvolved) image. If followed by 'PB', the image has been corrected for primary beam attenuation.
- 'SPX' denotes spectral index.
- 'DGP' denotes degree of polarization.
- 'POLA' and 'PANG' denote polarization angle.
- 'POLC' denote polarization fraction, corrected for Ricean bias.
- Numbers following these last four items give the permitted error threshold applied for blanking the output pixels.

All files end in '.1' – this is a sequence number and adds no additional information.

For example, 'U273ABC-1.4.UCLN' is a Stokes U clean image made with U band data, using the A, B, and C configurations, with 1.4 arcseconds resolution. 'UX273-1.4.SPX.1.1' is a spectral index image between U and X bands, with 1.4 arcseconds resolution, with an error threshold of 0.1 in spectral index. (All pixels with rms error greater than 0.1 are blanked). 'U273ABC-1.4.DGPSN3.1' is a fractional polarization image, at U-band, with 1.4 arcseconds resolution, blanked at a SNR of less than 3.

6. Conclusions

The Very Large Array has been utilized to generate high-fidelity radio images of the iconic quasar 3C273. Major features found by this work include:

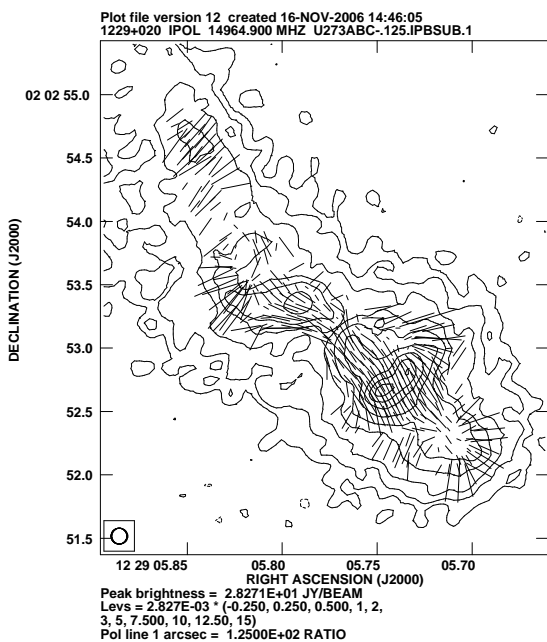


Fig. 13. The polarization structure of the outer jet at 14965 MHz, with 0.125 arcsecond resolution. The polarized emission from the more extended regions of the jet is not visible due to insufficient sensitivity.

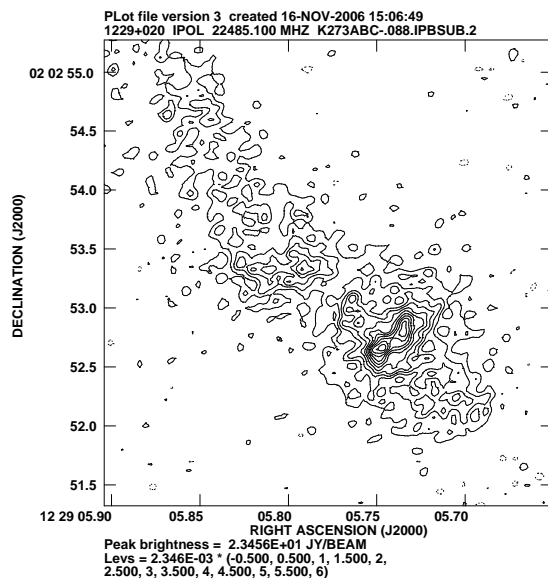


Fig. 14. The structure of the brightest hotspot at 22345 MHz, with 0.088 arcsecond resolution. The hotspot is now almost completely resolved out, indicating there are no physical structures less than ~ 300 pc in size.

- A previously unknown low-brightness steep-spectrum diffuse halo, of extent 30×45 arcseconds, primarily on the northern and western side of the bright nucleus and jet.
- A bright, narrow, nearly straight inner jet, of 11 arcseconds length, joining the bright nucleus to the outer jet. The transition in width from the narrow to wider jet is abrupt.
- The inner jet comprising three elongated regions of enhanced brightness, the outer two of which are oppositely tilted by about 5 degrees from the jet axis, suggestive of an oscillatory or sinusoidal underlying structure of period ~ 5 arcseconds.
- The outer jet, of width ~ 2.5 arcseconds, which also comprises an oscillatory structure, with a similar period, but significantly larger amplitude.
- The outer jet is highly linearly polarized, with the polarization fraction reaching 55% along the jet boundaries. The fractional polarization in the central regions of the outer jet is much lower. The projected magnetic field accurately follows the lines of constant brightness, including curling around the leading edge of the jet.
- The inner jet is also highly polarized, with the magnetic field lines oriented along the jet axis.
- The bright radio hotspot ‘H2’ is fully resolved with ~ 0.09 arcsecond (300 pc) resolution.
- The spectrum of the outermost regions of the radio jet sharply steepens above 5 GHz. The inner jet’s spectrum is flatter than that of the outer jet.
- The rotation measure of the jet is uniform, with no visible gradient either across or along the jet.

Despite the detailed information on the structure of this source provided by this work, much remains uncertain, or poorly determined. We note, in particular:

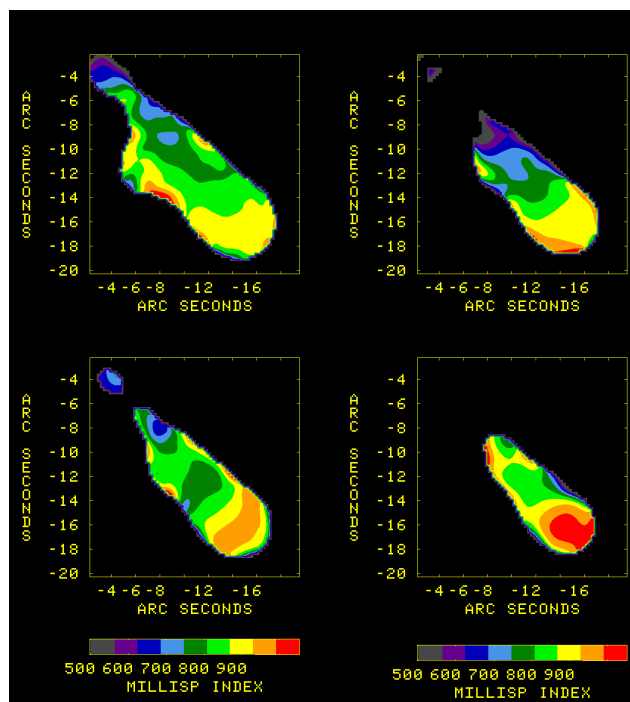


Fig. 15. A four-panel figure showing the change in spectral index through the centimeter radio band, at 2.0 arcseconds resolution. Upper left: α_{1365}^{4885} , Upper Right: α_{4885}^{8415} , Lower Left: α_{8415}^{14965} , Lower Right: α_{14965}^{22345} . These show the dramatic steepening of the spectrum in the region of the bright radio hot spot ‘H2’.

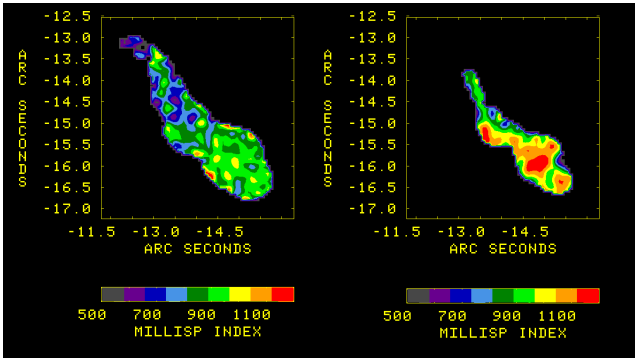


Fig. 16. A two-panel figure showing the change in spectral index through the centimeter radio band at 0.25 arcseconds resolution. Left: α_{8415}^{14965} , Right: α_{14965}^{22345} . These show the dramatic steepening of the spectrum in the region of the brightest radio hot spot ‘H2’ is not confined to the hotspot alone, but extends well beyond, in both directions.

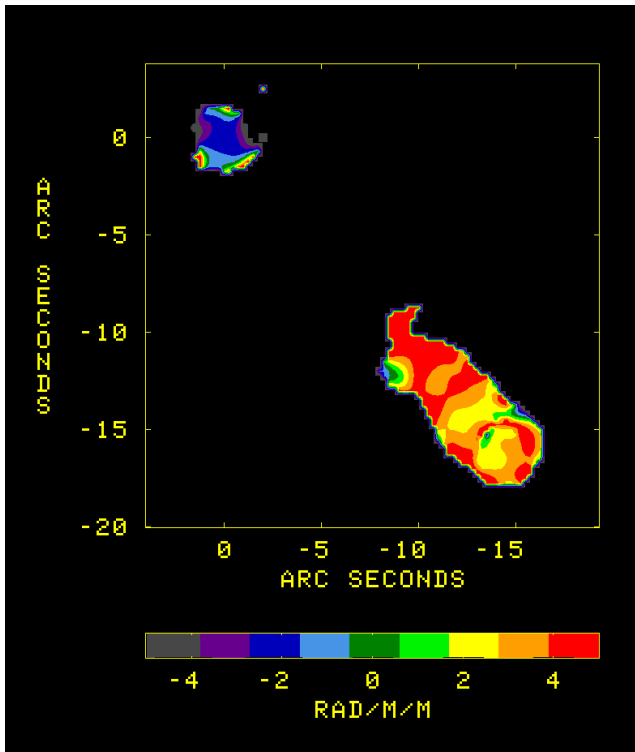


Fig. 17. The rotation measure as determined from the 1365 and 4885 MHz position angle images at 1.4 arcseconds resolution. The small-scale variations seen in both the jet and nucleus are artefacts from the noise. The jet has a uniform RM both across and along its axis.

- The structure of the newly-discovered halo is very uncertain. While we are confident in the existence of this emission, the differences in structures suggested by comparison of Figures 1 to 3 are unlikely to be real.
- The current images are noise limited at all the higher frequencies, particularly in polarization. Hence, details of the jet structure and polarization at high frequencies and at high resolution are poorly determined.
- The polarization of the inner jet is only approximately known, since the high-fidelity data taken in 1987 and 1991 were in a single-polarization mode.

The recent upgrade of the Very Large Array can address all these, and other issues. With the dramatic increase in bandwidth, im-

proved receiver sensitivities, and especially with the implementation of a much more powerful correlator, much superior imaging of this source – and other such sources – is easily in range.

Acknowledgements. RAP is pleased to acknowledge the generosity and hospitality of the Max-Planck Institut für Astronomie, and in particular that of Hermann-Josef Röser, during his many visits to Heidelberg, where most of this work was done. RAP also thanks Jean Eilek and Brian Punsly for helpful comments on the text.

References

- Baars, J.W.M., Genzel, R., Pauliny-Toth, I.I.K., & Witzel, A. 1977, *A&A*, 61, 99
- Conway, R.G., Garrington, S.T., Perley, R.A., and Biretta, J.A. 1993, *A&A*, 267, 347
- Davis, R.J., Muxlow, T.W.B., & Conway, R.G. 1985, *Nature*, 318, 343
- Jester, S., Röser, H.-J., Meisenheimer, K., and Perley, R. 2005, *A&A*, 431, 477
- Martel, A.R., Ford, H.C., Tran, H.D., Illingworth, G.D., Krist, J.E., White, R.L., Sparks, W.B., Gronwall, C., Cross, N.J.G., Hartig, G.F., Clampin, M., Ardila, D.R., Bartko, F., Benítez, N., Blakeslee, J.P., Bouwens, R.J., Broadhurst, T.J., Brown, R.A., Burrows, C.J., Cheng, E.S., Feldman, P.D., Franx, M., Golimowski, D.A., Infante, L., Kimble, R.A., Lesser, M.P., McCann, W.J., Menanteau, F., Meurer, G.R., Miley, G., Postman, M., Rosati, P., Sirianni, M., Tsvetanov, Z.I., and Zheng, W. 2003, *A.J.*, 125, 2964
- Perley, R.A., and Butler, B.J. 2013, *ApJS*, 19
- Punsley, B., and Kharb, P. submitted to *ApJL*.
- Schmidt, M. 1963, *Nature* 197, 1040
- Zavala, R.T., and Taylor, G.B. 2005 *ApJ*, 626, L73